

## Thermoelectric power of textured $\text{Bi}_2\text{Sr}_2\text{CaCu}_2\text{O}_8$ : Evidence for field-induced hysteretic behavior

S. Sergeenkov,\* M. Ausloos,<sup>†</sup> and H. Bougrine

*S.U.P.R.A.S., Institute of Physics, B5 University of Liège, Sart Tilman, B-4000 Liège, Belgium*

R. Cloots

*S.U.P.R.A.S., Institute of Chemistry, B6 University of Liège, Sart Tilman, B-4000 Liège, Belgium*

V. V. Gridin<sup>‡</sup>

*Department of Physics, University of Witwatersrand, Private Bag 3, P. O. Wits 2050, Johannesburg, South Africa*

(Received 3 February 1993; revised manuscript received 10 May 1993)

The thermoelectric power (TEP) of textured  $\text{Bi}_2\text{Sr}_2\text{CaCu}_2\text{O}_8$  has been measured with an ac technique in an applied magnetic field (up to 3 kG). Parallel and perpendicular geometries of the temperature gradient and the magnetic field have been systematically studied. A field-induced hysteretic behavior of the TEP due to the difference between cooling and heating runs is observed. The hysteresis surface versus field curve presents a maximum near 100 G for both geometries. The hysteretic behavior below  $T_c$  is discussed in terms of the intrinsic Josephson effect caused by the formation of Josephson vortices, while above  $T_c$  the hysteresis is attributed to the manifestation of the two-dimensional Gaussian fluctuations of the order parameter. In so doing, the critical-current density is found to behave as  $J_c \propto [1 + (H/H_J)^2]^{-1}$ . An activation energy,  $U(T, H)$ , deduced from the Arrhenius plot of the TEP below  $T_c$ , shows a linear temperature dependence,  $U(T) \approx 1 - T/T_c$ , a power-law magnetic field dependence,  $U(H) \propto H^{-1/4}$ , and has the absolute value of ca. 0.5 eV at  $T=0$  and  $H=50$  G. Such a behavior of the observed TEP and the dependences and origin of  $U(T, H)$  are argued to be attributed to the highly anisotropic nature of  $\text{Bi}_2\text{Sr}_2\text{CaCu}_2\text{O}_8$  layered superconductors.

### I. INTRODUCTION

The transport properties of high-temperature superconductors (HTS) are of great interest for their temperature and applied magnetic-field varied behavior, and constitute a fine test of the interplay between various scattering mechanisms. One of the most elusive transport properties is the thermoelectric power (TEP) which is an off-diagonal Onsager coefficient<sup>1</sup> and thus has to be treated in a more refined manner if some interpretation has to be given concerning its behavior. Furthermore, this is a quantity which has to be measured under well-defined conditions before data interpretation.

In superconductors the thermoelectric power is a fine probe of the superconductivity regime since the TEP is identical to zero in the coherent state. It is worthy to notice that the behavior of the TEP in the normal state of HTS is not yet completely explained,<sup>2,3</sup> and much controversy exists on its behavior near  $T_c$  with regards to the influence and the range of fluctuations.<sup>4</sup> Even the sign of the TEP tensor components of HTS is still somewhat undetermined.

In unsubstituted layered Bi-based HTS, the fluctuation effects have been clearly observed in transport properties like the conductivity,<sup>5-11</sup> and the thermoelectric power.<sup>12-14</sup> Some study of the fluctuations in the presence of fields have been recently reported, and have indicated the wide temperature range in which they can be seen.<sup>15-17</sup> In particular, the wide bump (often attributed to fluctuations<sup>2,3</sup>), seen above the critical temperature  $T_c$  in the case of YBCO systems, is not seen on Bi- (and Tl-)

based systems, though much of the behavior above  $T_c$  has to be attributed to fluctuation effects.<sup>4,18,19</sup> Often the shift of the zero value TEP can be monitored to define some critical temperature shift, mostly attributed to weak-link effects<sup>20,21</sup> or to vortex motion in the mixed state of type-II superconductor.<sup>22-24</sup> It is thus of great interest to reexamine the behavior of the TEP in layered HTS under well-defined conditions, and, in particular, in the presence of a magnetic field.

We report here on the longitudinal (along the CuO planes) magneto-TEP measurements of a textured polycrystalline  $\text{Bi}_2\text{Sr}_2\text{CaCu}_2\text{O}_8$  superconductor. Due to the highly textured nature of the sample the usual weak-link effects (due to intergranular grain boundaries) are essentially reduced.<sup>25</sup> Yet, we can expect the manifestation of the intrinsic Josephson effects (due to the layered nature of the sample used) as well as the enhancement of low-dimensionality contributions. Assuming that Josephson junctions lie in the  $a$ - $b$  plane, we have to distinguish carefully the Josephson effects in zero and nonzero (in the plane) magnetic fields. Namely, in contrast to the zero-field case (when a Josephson current indeed appears along  $c$  axis and thus may cause a transverse component to the TEP,<sup>20-22</sup> application of the magnetic field parallel to the junctions results in a more pronounced effect, i.e., the field modulation of the Josephson current  $J_c(H)$  in the  $a$ - $b$  plane [or along the  $x$  axis according to our geometry, see Eq. (6) below] thus contributing (chiefly) to the *longitudinal* part of the *magneto-TEP* of interest in this paper. Notice that it has been verified experimentally<sup>21</sup> that application of even a rather small field will drastically

reduce the *transverse* component of the TEP when a geometry other than the one described below is used.

Furthermore, the critical temperature (to be precisely defined below) is supposed to be higher than in YBCO systems, and therefore the fluctuation regime could be better seen as well. Both (Josephson weak-link and fluctuation) contributions are thus expected to be observable.

We have measured TEP along a pulse technique in a home-built experimental setup. We have observed that for such a textured sample the cooling and heating runs lead to hysteretic behavior in *nonzero* applied magnetic field. We have considered the two most symmetrical geometries, i.e., letting the thermal gradient and applied magnetic field be perpendicular or parallel. We have taken care of using the same systematic order of applied magnetic field strength during a cooling and heating run of the sample. As was observed in resistivity experiments<sup>26,27</sup> this “historical order” is of major importance in order to have some reproducible data.

The hysteresis surface versus field curve is found to present a maximum near 100 G. Below  $T_c$ , the obtained experimental data are discussed in terms of the so-called<sup>28,29</sup> “intrinsic Josephson effect” due to a weak coupling between double CuO layers when the field is applied along the *ab* plane. In so doing the critical-current density is found to behave like  $J_c \approx [1 + (H/H_J)^2]^{-1}$ . The hysteretic behavior observed above the critical temperature is related to the two-dimensional Gaussian fluctuations of the superconducting order parameter.<sup>19</sup> Furthermore, an Arrhenius plot of the magneto-TEP below  $T_c$  allows us to obtain the temperature,  $U(T) \approx (1 - T/T_c)$ , and field,  $U(H) \approx H^{-1/4}$ , dependences of the activation energy due to flux creep processes. We argue that these dependences can be attributed to anisotropic behavior of the layered superconductor with essentially different in-plane and out-of-plane penetration depths.<sup>16</sup>

## II. EXPERIMENTAL CONDITIONS

The Bi 2:2:1:2 sample has been cut from a 2:2:1:2 block prepared by the procedure described by Bock and Preisler.<sup>30</sup> Such a kind of sample has been thoroughly investigated by Doyle.<sup>25</sup> A scanning electron micrograph (SEM) of the sample is shown in Fig. 1. The analysis has been performed on the “pellet” surface. For so doing, a piece of the sample is embedded in epoxy resin, ground with SiC paper, and polished with diamond paste. We have successively observed the fractured and polished surface. The results reported in Fig. 1 are for the fractured surface. The sample consists of randomly oriented zones. Each zone is composed of large lamellar grains (single crystals) with an average size of 30–100  $\mu\text{m}$ , forming layers perpendicular to the *c* axis of the unit cell.

The sample ( $1.96 \times 1.73 \times 15.0 \text{ mm}^3$ ) has been placed in a home-built liquid- $\text{N}_2$  cryostat (in which a  $10^{-6}$ -Torr vacuum is obtained by a diffusion pump) and is mounted on a sample holder similar to that used in Ref. 31. A cylindrical copper block serves as a heat bath, controlled by a heater  $H_2$ , the temperature of which is regulated (between 4.2 and 300 K) through a Lake Shore temperature controller after measuring the temperature by a silicon

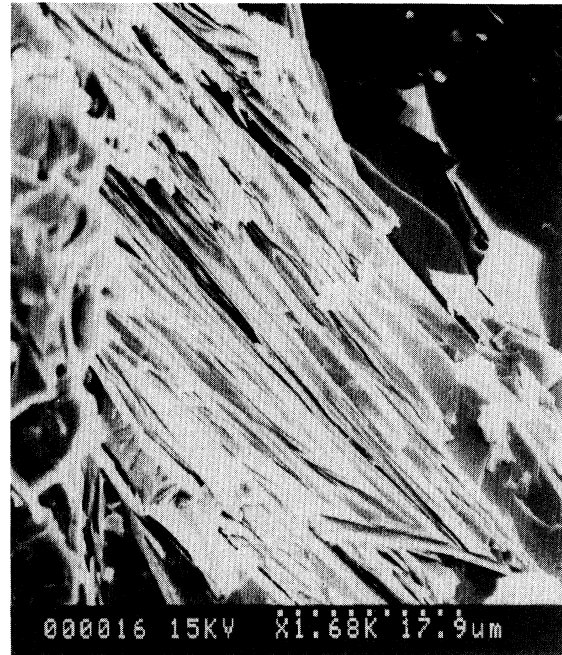


FIG. 1. Scanning electron micrograph of the textured  $\text{Bi}_2\text{Sr}_2\text{CaCu}_2\text{O}_8$  sample.

diode. The lower part of this copper block supports one end of the sample [Fig. 2(a)], the absolute temperature of which is measured by a carbon-glass resistance (CGR). Heat pulses are sent at the unsupported extremity of the sample through 80- $\mu\text{m}$ -diam noninductively wound constantan wires around the sample. The TEP is measured with two Cu-Ct thermocouples [*EF*, *ED*, *BC*, and *BA* wires in Figs. 2(a) and 2(b)], of 80  $\mu\text{m}$  in diameter for a distance  $EB \approx 5 \text{ mm}$ , from which, by appropriate numerical analysis, the sample TEP is deduced (the Appendix). The pulses are characterized by a 19.8-mA current passing through a 20- $\Omega$  resistance glued upon the sample end. This gives rise to about 1-K temperature difference. Heat pulses last 1 min and are followed by a 3-min waiting time after which the bath temperature is raised (or lowered) by about 0.7 K. (Such time lapses can be varied if necessary.) The data are averaged over four measurements taken during the last seconds of the heating pulse. The temperature of the sample is measured as the average between the hot and cold junctions (the Appendix). The range of  $T$  which has been specifically examined goes between 77 and 180 K, but the data are shown for the interesting region near the critical temperature only. The TEP is given as the ratio of  $\Delta V_{CD}/\Delta T_{EB}$ , with the denominator being deduced from  $\Delta V_{CD}$  and  $\Delta V_{AF}$  contributions. Such potential differences are of the order of 10  $\mu\text{V}$  for  $\Delta V_{CD}$  and 40  $\mu\text{V}$  for  $\Delta V_{AF}$  and measured with a Keithley nanovoltmeter linked to a Keithley multichannel switch. All instruments are PC controlled and monitored.

The magnetic field is generated by two Fe bars inserted into copper coils. They are mounted on a platform which can rotate around a vertical axis. A 3-kG field can be generated with a 3-A current. In all the cases reported

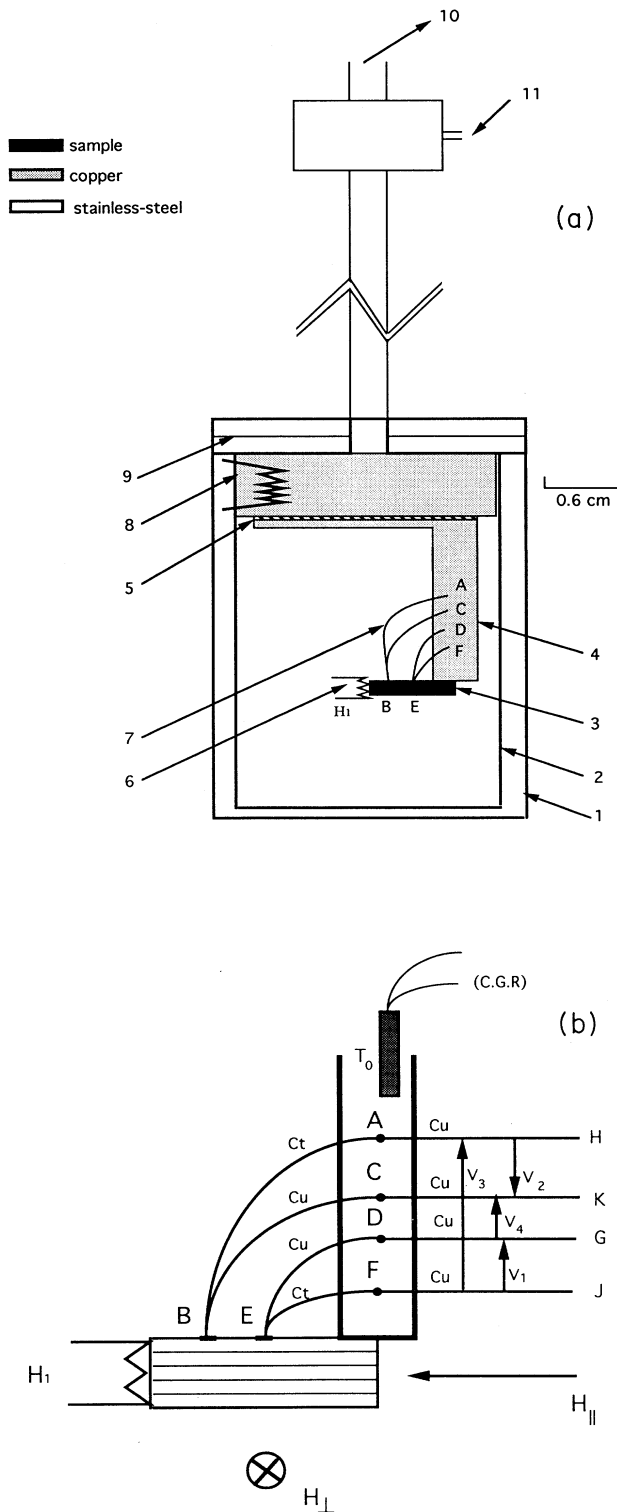


FIG. 2. (a) Experimental setup used for the measurements of the TEP: (1) protection lid, (2) radiation shield, (3) sample, (4) sample holder, (5) GE 7031 electrically insulating layer, (6) heater, (7) thermocouples, (8) heat bath with heater ( $H_2$ ) (9) Wood metal solder, (10) vacuum pump, (11) exit for measurement wires. (b) Side view of the sample holder showing the field and temperature gradient relative directions.

here the field has been applied parallel to the sample layers. The field has been applied in an increasing order when the field is parallel to the temperature gradient, and in a decreasing order when the field is perpendicular to the temperature gradient [Fig. 2(b)]. The field values have been 0, 50, 100, 750, 1000, 2000, and 3000 G.

### III. EXPERIMENTAL RESULTS

The zero-field temperature  $T$  dependence of the TEP, for  $T$  between 115 and 93 K is shown in Fig. 3. The TEP is positive and smoothly varying. The order of magnitude ( $5 \mu\text{V/K}$ ) is that found in the literature, see, e.g., Ref. 32 where Crommie *et al.* have measured similar systems to ours (before and after annealing in oxygen flow). They have observed that the pretreated (poorly oxygenated) sample has a TEP of the order of  $17 \mu\text{V/K}$  near its maximum, but the well-oxygenated sample has a TEP of the order of  $3 \mu\text{V/K}$ . The samples can be distinguished by their electrical resistivity which is markedly semiconducting in the pretreated case of Ref. 32. Our sample is not semiconducting-like. Since the sample might not be as well oxygenated as the best sample of Crommie *et al.*, a difference of a couple of  $\mu\text{V/K}$  is therefore not unlikely. Thus, we may consider that the "factor of 2" variation in the order of magnitude is likely due to a different oxygen content.

As usual,<sup>33</sup> a quasilinear downward behavior has been observed at high temperature. An important feature for TEP is the slope at "high" temperature: it is a measure of the Fermi energy (or Fermi temperature) of the sample. We have the same order of magnitude as Crommie *et al.*, i.e.,  $0.03 \mu\text{V/K}^2$ .

Notice the absence of the hysteretic behavior between heating up and cooling down regimes in zero field. A typical field behavior of the magneto-TEP for magnetic field  $H=750$  G and for two geometries outlined on the graphs is given in Fig. 4. The field-induced hysteretic behavior of the TEP produced by the difference between cooling,  $S_c(T, H)$ , and heating,  $S_h(T, H)$ , runs is clearly

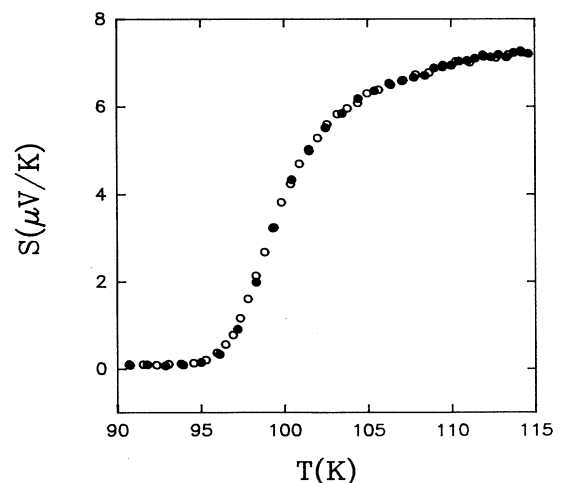


FIG. 3. Temperature dependence of the TEP at  $H=0$  for cooling (open symbols) and heating (solid symbols) runs. Hereafter the error bars are of a size comparable to the symbols.

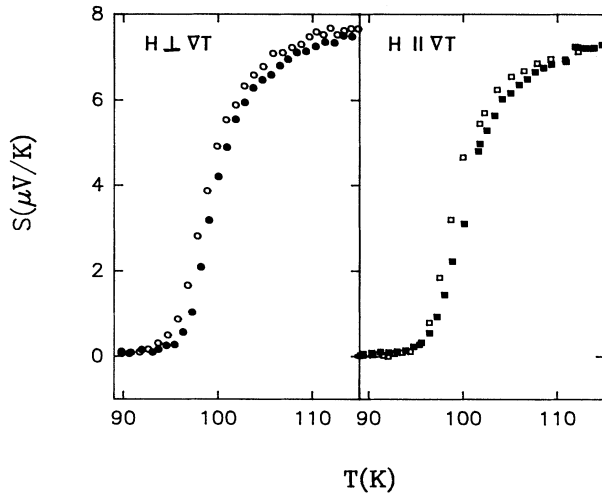


FIG. 4. Temperature dependence of the TEP at  $H = 750$  G for  $\nabla T \perp H$  (left) and  $\nabla T \parallel H$  (right) configurations.

seen. We have observed the hysteresis surface,  $A(H) = \int_{T_1}^{T_2} dT \Delta S(T, H)$ , where  $\Delta S(T, H) = S_c(T, H) - S_h(T, H)$ , between an offset temperature ( $T_1$ ),  $\sim 10$  K below  $T_c$ , and an upper temperature ( $T_2$ ),  $\sim 15$  K above  $T_c$ . Such a surface (measured in  $\mu\text{V}$ ) is shown as a function of field in Fig. 5 for the parallel and perpendicular geometries.

For further discussion, the critical temperature should in principle be well defined, if possible from the statistical mechanics point of view. The latter defines  $T_c$  as that temperature at which the coherence length measuring the extent of the correlation function of a one-component order-parameter physical process goes to infinity.<sup>34</sup> It is then easy to show that this occurs at phase transitions like the superconducting one, or the magnetic ones,<sup>35</sup> when the Onsager transport coefficients have an inflexion

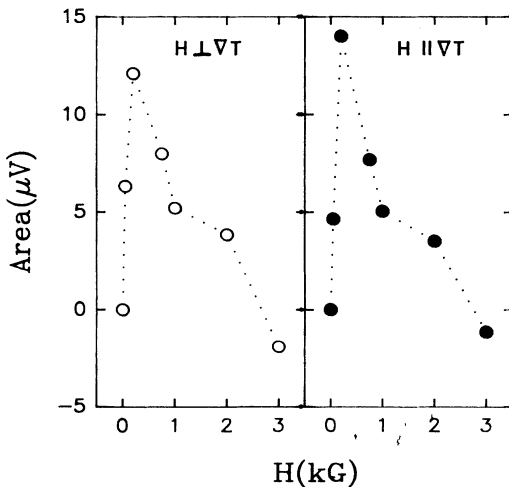


FIG. 5. The total hysteresis area (see text) as a function of applied magnetic field for both configurations (see Fig. 4). (Field data points are 0, 50, 100, 750, 1000, 2000, and 3000 G.)

point. Hence the first temperature derivative seems to go to “infinity.” Therefore, we have always used for the critical temperature that when  $dR/dT$  or  $dS/dT$  diverges.<sup>4</sup> This is indeed the temperature at which the grains become superconducting throughout. (There might be some distribution of critical temperatures because the grains are not all exactly the same, but this only leads to a broadening of the transition, and to not so well-defined critical exponents.<sup>4</sup>)

In polycrystalline materials another (geometrical) “phase transition” occurs: it is the “percolation transition” when the phases of the order parameter in each grain match each other across the weak links. This is when  $R$  and  $S=0$ , at  $T_R$  or  $T_p$  or  $T_0$  according to the notations. This occurs much below the official (legal)  $T_c$ .

Another “critical temperature” is sometimes met; let us call it  $T_{c0}$ . It corresponds to an extrapolation temperature concerning the *mean-field* behavior law in the vicinity of  $T_c$ . Its real physical validity is unclear (though it is often used).<sup>4</sup> It is rather a fit parameter, and corresponds to no experimental point. It can be estimated by Azlamazov-Larkin fluctuation terms for conductivity and TEP.<sup>4,36,37</sup>

To get as much interesting information from our experimental data as possible, we provide a separate fitting of the hysteresis surface,  $A(H) = A_{av}(H) + A_{fl}(H)$ , below  $T_c$  and above  $T_c$ , where

$$\begin{aligned} A_{av}(H) &= \int_{T_1}^{T_c} dT \Delta S(T, H), \\ A_{fl}(H) &= \int_{T_c}^{T_2} dT \Delta S(T, H). \end{aligned} \quad (1)$$

There is a shift of the critical temperature with the field, of course, but it is hardly noticed in the range of field with which we are concerned. ( $T_c$  shifts down by about 1 K per T.<sup>37</sup>)

Divided by the applied magnetic field, these two contributions are found to obey the following fitting expressions (see Figs. 6 and 7):

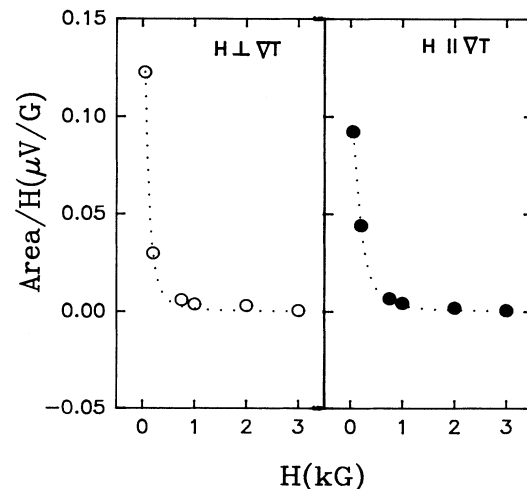


FIG. 6. Hysteresis area below  $T_c$  divided by  $H$  for two configurations (see Fig. 4) fitted by the function given in Eq. (2).

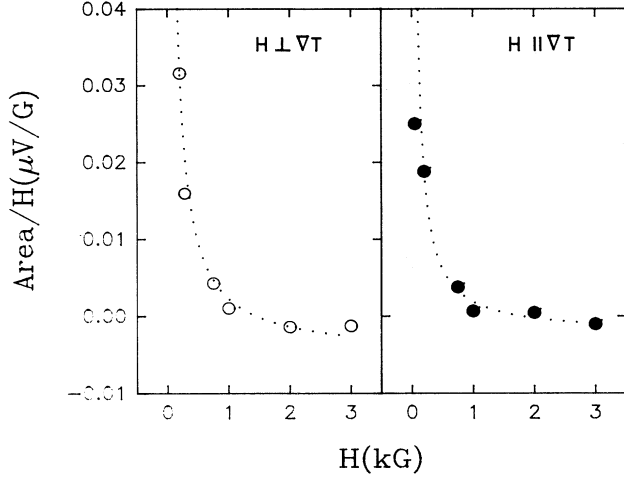


FIG. 7. Hysteresis area above  $T_c$  divided by  $H$  for two configurations (see Fig. 4) fitted by the function given in Eq. (3).

$$\frac{A_{av}}{H} = \frac{a}{1+bH^2}, \quad (2)$$

$$\frac{A_{fl}}{H} = \frac{c}{H} - d, \quad (3)$$

for which the parameters  $a$ ,  $b$ ,  $c$ , and  $d$  are given in Table I. Notice that the “fluctuation” contribution to the TEP hysteresis [Eq. (3)] changes its sign in the field region above 2 kG (see Fig. 7).

It is worthwhile to notice that the TEP and the resulting integral error bars do not play a dramatic role in the numerical analysis. Suppose indeed that we take 100 K as the critical temperature. The error on the integrated surface  $A$  is (100–99) K times the size of the TEP, i.e., of the order of  $4 \mu\text{V}/\text{K}$ , thus of the order of  $4 \mu\text{V}$  for the worse case (near 100 G). Even though this is not a negligible difference for the area versus field (Fig. 5), it obviously leads to a weak effect for the theoretical-numerical analysis of Figs. 6 and 7. Indeed the (area/ $H$ ) value at low field is then pushed up on an asymptotic curve without any change in the fitting parameters, whatever the geometry. On the other hand, at large field, the area becomes smaller, and the (area/ $H$ ) value is changed in a very minor way, smaller than the size of the data point. Therefore, the value which is used for  $T_c$  in the integral is marginally unimportant (as long as it is not ridiculously taken outside the physical range admissible of course).

For completeness, an Arrhenius plot (below  $T_c$ ),  $S(T, H) = S_0 \exp[-U(T, H)/k_B T]$ , of the TEP, extracted from Fig. 4, is depicted in Fig. 8. The fits are those for which the error bar on the final result is the minimum

TABLE I. Fitting parameters for perpendicular ( $\nabla T \perp H$ ) and parallel ( $\nabla T \parallel H$ ) configurations.

	$a$ ( $\mu\text{V}$ )	$b$ ( $\text{G}^{-2}$ )	$c$ ( $\mu\text{V}$ )	$d$ ( $\mu\text{V}/\text{G}$ )	$A_0$ ( $\text{eV G}^{1/4}$ )
$H \perp \nabla T$	0.15	$1 \times 10^{-4}$	7.25	$5 \times 10^{-3}$	0.65
$H \parallel \nabla T$	0.09	$3 \times 10^{-4}$	4.22	$2 \times 10^{-3}$	0.82

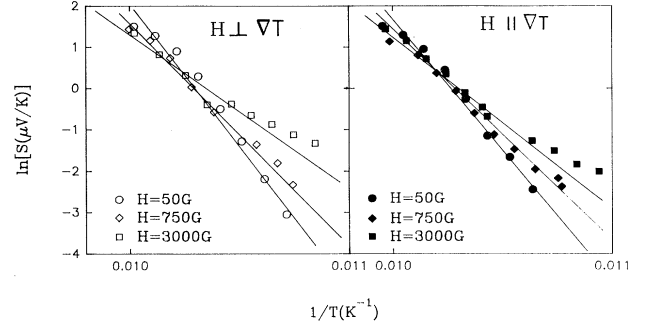


FIG. 8. Arrhenius plot of the TEP (heating run) for various magnetic fields and for both configurations (see Fig. 4). The solid line is a linear fit to the  $T < T_c$  temperature values.

one (of the order of 10% in the worse case). It is not small; however, such is always the case in  $1/T$  plots when the original data have some noise. The activation energy,  $U(T, H)$  (see Fig. 9), is found to be remarkably well fitted by the following temperature- and field-dependent law,  $U(T, H) = U(0, H)(1 - T/T_c)$ , with  $U(0, H) = A_0 H^{-1/4}$ . The absolute value of the activation energy at  $T=0$  and  $H=50$  G is  $U_{\perp} = 0.42$  eV and  $U_{\parallel} = 0.52$  eV for the perpendicular and parallel configurations, respectively. The fitting parameter,  $A_0$ , for both geometries used is given in Table I. Notice that a similar field dependence and the absolute value of the activation energy has been reported earlier for Bi 2:2:1:2 single crystals<sup>38</sup> and for Bi 2:2:2:3 polycrystals.<sup>39</sup>

#### IV. THEORETICAL INTERPRETATION

The magnetic-field-induced nature of the TEP hysteresis,  $\Delta S(T, H)$ , observed in our experiments, allows us to use the analogy with the well-known<sup>14,17,21,23</sup> hysteretic behavior of the irreversible magnetization (due to flux

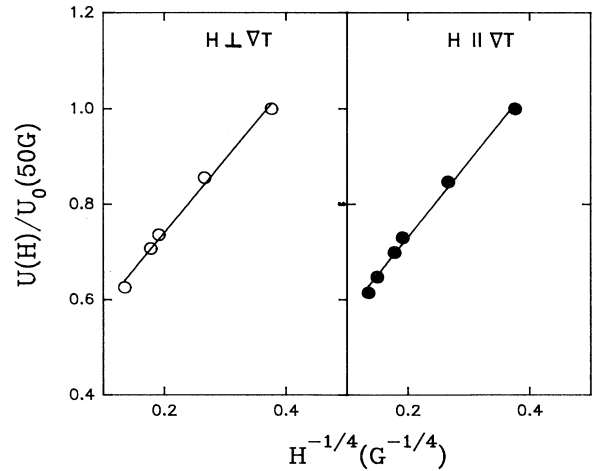


FIG. 9. Activation energy  $U(T, H)/U_0(T, 50 \text{ G})$  vs magnetic field for both configurations (see Fig. 4) determined from the Arrhenius plot (Fig. 8) and fitted by the power-law function  $H^{-1/4}$ .

motion),  $\Delta M(T, H)$ , of type-II superconductors. Indeed, the magneto-TEP of such a superconductor in the mixed state,  $S(T, H)$ , is related to the transport entropy,  $\sigma(T, H)$ , in the way<sup>1,17</sup>  $S(T, H) = (H/ne\Phi_0)\sigma(T, H)$ , where  $n$  is the total carrier density,  $e$  is the electron charge, and  $\Phi_0$  is the flux quantum. In turn, the transport entropy is related to the irreversible magnetization,  $M(T, H)$ , as follows,<sup>17</sup>  $\sigma(T, H) = \Phi_0 \partial M(T, H) / \partial T$ . As a result, we get the following relation between the hysteresis of magnetization,  $\Delta M(T, H)$ , and the corresponding hysteresis of magneto-TEP,  $\Delta S(T, H)$ :

$$\Delta S(T, H) = \frac{H}{en} \frac{\partial \Delta M(T, H)}{\partial T}. \quad (4)$$

Since the hysteretic behavior of the TEP has been observed both below and above  $T_c$ , it seems reasonable to treat these temperature intervals separately, attributing the regions  $(T_1, T_c)$  and  $(T_c, T_2)$ , respectively, to the “average” value,  $A_{av}(H)$ , and the “fluctuation” contribution,  $A_{fl}(H)$ , of the field-dependent hysteresis area  $A(H) = A_{av}(H) + A_{fl}(H)$ , where  $A_{av}(H)$  and  $A_{fl}(H)$  are given by Eq. (1). Making use of the Bean relation between the irreversible magnetization and the critical-current density,  $\Delta M(T, H) = J_c(T, H)D$ , where  $D$  is the sample thickness, Eqs. (1) and (3) result in the following relation between the average critical current density in the  $ab$  plane (see below) and the “average” hysteresis area

$$J_c(H) \equiv J_c(T_1, H) = \frac{en}{D} \left[ \frac{A_{av}(H)}{H} \right] = \frac{J_c}{1 + (H/H_J)^2}. \quad (5)$$

Here  $J_c = ena/D$ ,  $(H_J)^2 = 1/b$ , where  $a$  and  $b$  are the fitting parameters (see Table I), and to get the last expression in the rhs of Eq. (5), the fitting function for  $A_{av}(H)$  [see Eq. (2)] has been used. Using for the carrier density<sup>40</sup>  $n = 5 \times 10^{27} \text{ m}^{-3}$ , and taking into account the sample size (thickness)  $D = 1.8 \text{ mm}$  and the value of the fitting parameters  $a_{\perp}$ ,  $a_{\parallel}$ ,  $b_{\perp}$ , and  $b_{\parallel}$  (see Table I), for the estimate of the critical-current density,  $J_c$ , and the characteristic field,  $H_J$ , deduced from the parallel and perpendicular geometries, we get  $J_{c\parallel} = 2 \times 10^3 \text{ A/cm}^2$  and  $H_{J\parallel} = 170 \text{ G}$ , and  $J_{c\perp} = 5 \times 10^3 \text{ A/cm}^2$  and  $H_{J\perp} = 100 \text{ G}$ , respectively.

According to Eq. (5), the field dependence of the critical-current density indicates a weak-link limited behavior. Since the textured character of our sample reduces the possibility of grain boundary weak links, we arrive at the conclusion that the above behavior of  $J_c(H)$  can be attributed to the so-called “intrinsic Josephson effect,” proved<sup>28,29,41</sup> to be active in layered superconductors with the Josephson-like coupling between layers. (Recall that the heater has some finite thickness along the  $c$  axis.)

Indeed, let us consider a layered superconductor as a stack of double CuO planes separated by a distance  $s$  ( $s = 12 \text{ \AA}$  in  $\text{Bi}_2\text{Sr}_2\text{CaCu}_2\text{O}_8$ ).<sup>9</sup> When the length  $L$  of a single Josephson junction (JJ), normal to the applied magnetic field (and thus corresponding to the largest “grain” size), is much less than the Josephson penetration depth  $\lambda_J$  [which is defined via the Josephson critical current density,  $J_0$  as  $(\lambda_J)^2 = \Phi_0 / 2\pi\mu_s J_0$ ], so that  $H \gg H_J = \Phi_0 / 2\pi s \lambda_J$ , the current density through a sin-

gle JJ contact is defined by the well-known<sup>39</sup> Josephson relation  $J(x) = J_0 \sin\phi(x)$ , where the local change of the phase of the order parameter reads  $\phi(x) = \phi(0) + 2\pi s x H / \Phi_0$ . In the opposite case of large JJ contacts, when  $\lambda_J \ll L$ , the above current density is caused by the creation of Josephson vortices, so that  $J(x) \approx \exp(-x/\lambda_J)$ . Thus, in general, the maximum critical current density in the  $ab$  plane via single JJ contact can be presented in the form<sup>42</sup>

$$J_c(H) \equiv \frac{1}{L} \int_0^L dx J(x) = \frac{1}{L} \int_0^L dx J_0 \exp(-x/\lambda_J) \cos \left[ \frac{2\pi H s x}{\Phi_0} \right]. \quad (6)$$

It is easy to check that in the limit of small JJ contacts, when  $\lambda_J \gg L$ , Eq. (6) reduces to the well-known Fraunhofer-like pattern

$$J_c(H) = J_0 \left| \frac{\sin(H/H_0)}{(H/H_0)} \right|, \quad H_0 = \Phi_0 / 2\pi s L, \quad (7)$$

while in the opposite limit, when  $\lambda_J \ll L$ , Eq. (6) reads [cf. Eq. (5)]

$$J_c(H) = \frac{J_c}{1 + (H/H_J)^2}, \quad J_c = (\lambda_J/L) J_0. \quad (8)$$

Equations (6)–(8) describe the field modulation of Josephson current in the  $a$ - $b$  plane only. And this is the only possibility when  $H$  is quasi in the  $a$ - $b$  plane, as expected in our geometry. Some mild misorientation leads to some hard to estimate contribution from the transverse component, but likely to be quite negligible in the range of field which is investigated.<sup>21</sup>

Thus, according to our experimental observations, in the examined case, the critical-current density is limited by the Josephson vortices, occurring between CuO planes. Furthermore, using the above-mentioned experimental values for  $H_J$  and  $J_c$ , we get the following estimates for the average JJ length  $L$  and the Josephson penetration depth  $\lambda_J$ , namely  $L = 100 \text{ nm}$  and  $\lambda_J = 20 \text{ nm}$ , which give for the Josephson current density [see Eq. (8)]  $J_0 = 5J_c$ . It is worthwhile to notice that the Josephson vortices limited behavior of  $J_c(H)$  [given by Eq. (8)] has been observed<sup>43</sup> also in heavily irradiated  $\text{Bi}_2\text{Sr}_2\text{CaCu}_2\text{O}_8$  single crystals when the magnetic field is applied along the irradiation-induced columnar defects. At the same time, the unirradiated  $\text{Bi}_2\text{Sr}_2\text{CaCu}_2\text{O}_8$  single crystals were found<sup>29</sup> to exhibit a more recognized Fraunhofer-like pattern [see Eq. (7)]. We infer that a similar field dependence of the critical-current density for irradiated single crystals and textured materials is not an accident because in both cases an extended boundary (tracks of damaged material or interfaces between layers) creates a JJ contact and simultaneously produces a direction of preferential pinning (see below).

Turning to the contribution above  $T_c$ ,  $A_{fl}(H)$  [see Eq. (3)], we show that this contribution can be attributed to the manifestation of strong two-dimensional (2D) Gaussian fluctuations of the order parameter in layered super-

conductor.<sup>19</sup> As it is well known,<sup>35</sup> the Gaussian fluctuations of any observable quantity which is conjugated to the order parameter  $\psi$  can be represented in terms of the statistical average of the square of the fluctuation amplitude,  $\langle |\delta\psi|^2 \rangle$ , with  $\delta\psi = \psi - \psi_0$ , where  $\psi_0$  is the mean value of the order parameter defined as the stable solution of the equation  $\delta\mathcal{F}/\delta|\psi| = 0$ . In the mixed state of type-II superconductor the free-energy density functional,  $\mathcal{F}$ , in the external magnetic field,  $H$ , reads<sup>17,19</sup>

$$\mathcal{F} = \mathcal{F}_n + \alpha(T)|\psi|^2 + \frac{\beta}{2}|\psi|^4 + MH. \quad (9)$$

Hereafter  $|\psi|^2$  is the space-averaged order parameter,  $\alpha(T) = \alpha_0(T - T_c)$ ,  $\alpha_0 = 1.83\hbar^2/2m^*s^2T_c$ , where  $m^*$  is an effective mass (see below), and  $\beta = \alpha_0T_c/2n_s$ , where  $n_s$  is the number density of the superconducting carriers at  $T=0$ ; the subscripts  $s$  and  $n$  refer to superconducting and normal components, respectively. The magnetization,  $M$ , in Eq. (9) designates the magnetization of the Abrikosov vortex lattice defined via the space-averaged order parameter as<sup>44</sup>  $M = (B - H)/4\pi = -\mu_B|\psi|^2$ , where  $\mu_B = e\hbar/2m_e$  is the Bohr magneton. The fluctuations of the TEP above  $T_c$  have the form (cf. Ref. 19)

$$\Delta S_{\bar{n}}(T, H) = C(H)\langle |\delta\psi|^2 \rangle, \quad (10)$$

where

$$\begin{aligned} \langle |\delta\psi|^2 \rangle &= \int d\psi |\delta\psi|^2 \\ &\times \exp(-\Delta\mathcal{F}/k_B T) / \int d\psi \exp(-\Delta\mathcal{F}/k_B T). \end{aligned} \quad (11)$$

Here  $\Delta\mathcal{F} = \mathcal{F} - \mathcal{F}_0$ ,  $\mathcal{F}_0 = \mathcal{F}(\psi_0)$ , and the coefficient  $C(H)$  will be defined below. Expanding the free-energy functional  $\mathcal{F}$  around the mean value of the order parameter,  $\psi_0$ , namely,

$$\mathcal{F}(\psi) \cong \mathcal{F}(\psi_0) + \frac{1}{2} \left[ \frac{\partial^2 \mathcal{F}}{\partial |\psi|^2} \right]_{|\psi| = |\psi_0|} (\delta\psi)^2 \quad (12)$$

we can calculate the Gaussian integrals [Eq. (11)] explicitly, and making use of the fact that above  $T_c$  the mean value of the order parameter  $\psi_0 = 0$ , we obtain for  $\Delta S_{\bar{n}}(T, H)$  (Ref. 19) [see Eq. (9)]

$$\Delta S_{\bar{n}}(T, H) = \frac{C(H)k_B T_c}{2\alpha_0(T - T_c) - 2\mu_B H}. \quad (13)$$

To determine the form of the coefficient  $C(H)$ , we assume that, at  $T = T_c$ ,  $|\Delta S_{\bar{n}}(T_c, H)| = |\Delta S_{\text{exp}}(T_c, H)|$ , where  $\Delta S_{\text{exp}}(T_c, H)$  is the experimental value of the TEP hysteresis surface at  $T_c$ . The coefficient  $C(H)$  then has the form

$$C(H) = \left[ \frac{2\mu_B H}{k_B T_c} \right] \Delta S_{\text{exp}}(T_c, H). \quad (14)$$

Finally, using Eqs. (1), (13), and (14), the ‘‘fluctuation’’ contribution to the TEP hysteresis area,  $A_{\bar{n}}(H)$ , reads

$$\begin{aligned} A_{\bar{n}}(H) &\equiv \int_{T_c}^{T_2} dT \Delta S_{\bar{n}}(T, H) \\ &= \left[ \frac{\mu_B H \Delta S_{\text{exp}}(T_c, H)}{\alpha_0} \right] \ln \left| \frac{\alpha_0(T_2 - T_c) - \mu_B H}{\mu_B H} \right|. \end{aligned} \quad (15)$$

Since within the field region used in our experiments  $1 < \alpha_0(T_2 - T_c)/\mu_B H \leq 2$ , we can expand the logarithm in Eq. (15) and get, with good accuracy,

$$\frac{A_{\bar{n}}}{H} = \frac{c}{H} - d \equiv \left[ \frac{H^*}{H} - 1 \right] d \quad (16)$$

in agreement with the fitting equation (3). Here  $c = (T_2 - T_c)\Delta S_{\text{exp}}(T_c, H)/\mu_B$ ,  $d = 2\mu_B \Delta S_{\text{exp}}(T_c, H)/\alpha_0$ , and  $H^* = c/d = \alpha_0(T_2 - T_c)/2\mu_B$ . Notice that in contrast to the coefficients  $c$  and  $d$ , the characteristic field  $H^*$  does not contain the experimentally dependent parameter  $\Delta S_{\text{exp}}(T_c, H)$ . Using the experimental values of the parameters  $c$ ,  $d$ ,  $T_c$ , and  $T_2$  (see Table I), we get the following estimates:  $\Delta S_{\text{exp}}(T_c, H) = 0.4 \mu\text{V/K}$ ,  $H^* = 2 \text{ kG}$  (both agree well with our data), and  $\alpha_0 = 2.5 \times 10^{-25} \text{ J/K}$ . Furthermore, the found value of the latter parameter,  $\alpha_0$ , allows us to estimate the  $ab$ -plane effective mass,  $m_{ab}^*$ , of the superconducting carriers in layered  $\text{Bi}_2\text{Sr}_2\text{CaCu}_2\text{O}_8$ . Indeed, according to the above-given definition [see Eq. (9)], the effective mass<sup>45</sup>  $m^* = (m_{ab}^* m_c^*)^{1/2} = \gamma m_{ab}^*$ , where  $\gamma = (m_c^*/m_{ab}^*)^{1/2}$  is the so-called anisotropy parameter, can be expressed via  $\alpha_0$  as  $m^* = 1.83\hbar^2/2\alpha_0 s^2 T_c$ . Using the above value of  $\alpha_0$ , and taking into account that in  $\text{Bi}_2\text{Sr}_2\text{CaCu}_2\text{O}_8$  (Ref. 45)  $s = 12 \text{ \AA}$  and  $\gamma = 55$ , we get  $m_{ab}^* \approx 8m_e$  in a good agreement with the reported data for this parameter.<sup>3,19</sup>

An Arrhenius plot is not usual for TEP but is presented here for explaining the finite value of  $S(H, T)$  below  $T_c$ . (A similar plot has already been presented by Dascalidou *et al.*,<sup>39</sup> but without interpretation.) One argument for such a plot originates in the fact that the magneto-TEP is similar for thermal transport processes to the magnetoresistance (for electrical processes) which shows activation (flux-creep) energy on such plots: see, e.g., Fig. 2 in the often quoted letter of Palstra *et al.*<sup>38</sup>

A possible interpretation of the temperature and field dependence of the activation energy,  $U(T, H)$ , deduced from an Arrhenius plot (see Figs. 8 and 9) of the TEP,  $S(T, H) = S_0 \exp[-U(T, H)/k_B T]$ , is of interest and in order. We argue that the observed behavior,  $U(T, H) = A_0(1 - T/T_c)H^{-1/4}$ , results from weak pinning of 2D ‘‘pancake’’ vortices by interfaces in textured  $\text{Bi}_2\text{Sr}_2\text{CaCu}_2\text{O}_8$ . (It is worthy to recall that a similar behavior has been found<sup>43</sup> also in irradiated  $\text{Bi}_2\text{Sr}_2\text{CaCu}_2\text{O}_8$  single crystals when the magnetic field is applied along the track of damaged material to get as large pinning as possible.)

In the configuration  $H \parallel ab$  vortices are the Josephson ones. An energetically favorable way for these vortices to pass from one interlayer position to the next can be provided by the nucleation of ‘‘pancake’’ vortex-antivortex

pairs, which are driven apart by the Lorentz force (if an electric transport current is applied) or by its analog, the thermal force (induced by an applied thermal gradient).<sup>39</sup> Although in our experiments the field is supposed to be applied along the  $ab$  plane of the sample, it is practically impossible to avoid its penetration along the  $c$  axis as well. As it was found<sup>29</sup> even a rather small misorientation of the field from the  $ab$  plane (less than  $1^\circ$ ) results in a finite density of “pancake” vortices between layers. As is known, when a superconductor contains nonsuperconducting regions, the fluxoids can lower their energy by interacting with such regions. The energy gain per interaction is<sup>46,47</sup>

$$U(T, H) = \frac{1}{2\mu_0} B_c^2(T) V(T, H). \quad (17)$$

Here  $B_c(T) = \Phi_0 / 2\sqrt{2}\pi\lambda(T)\xi(T)$  is the thermodynamic critical field of the superconductor, where  $\lambda(T) = \lambda(0)(1 - T/T_c)^{-1/2}$  and  $\xi(T) = \xi(0)(1 - T/T_c)^{-1/2}$  are the London penetration depth and the coherence length, respectively, and  $V(T, H)$  is the interaction volume. In the case of large nonsuperconducting regions (e.g., irradiation-induced tracks or interfaces in textured sample), the energy change occurs only at the interfaces. In small fields,  $H \ll H_d$ , where  $H_d \propto \Phi_0 / (d_p)^2$  is a characteristic field defined via the distance between defects,  $d_p$ , all vortices are pinned, and  $V(T, H) = \pi\xi^2(T)a_0(H)$ , where  $a_0(H) = (\Phi_0/H)^{1/2}$  is the vortex spacing. In high fields,  $H \gg H_d$ , all the pinning sites are occupied so that  $d_p > a_0(H)$  and  $V(T, H) = \pi\xi^2(T)d_p$ . Due to the highly anisotropic nature of the layered  $\text{Bi}_2\text{Sr}_2\text{CaCu}_2\text{O}_8$ , the activation energy of this superconductor is  $U = (U_{ab}U_c)^{1/2}$ , where  $U_{ab}$  and  $U_c$  are the in-plane and out-of-plane activation energies, respectively, with  $\xi^2 = \xi_{ab}\xi_c$  (and  $\lambda^2 = \lambda_{ab}\lambda_c$ ). Remarkably, the large anisotropy ratio between penetration depths,  $\lambda_c = \gamma\lambda_{ab}$  ( $\gamma = 55$  in  $\text{Bi}_2\text{Sr}_2\text{CaCu}_2\text{O}_8$ ),<sup>45</sup> results in different forms of in-plane ( $V_{ab}$ ) and out-of-plane ( $V_c$ ) interaction volumes  $V = (V_{ab}V_c)^{1/2}$  according to the above scenario. Indeed, for an applied field  $H$  such that  $H_{c1,c} \ll H \ll H_{c1,ab}$ , where  $H_{c1} \propto \Phi_0/\lambda^2$  with appropriate penetration depth ( $\lambda_{ab}$  or  $\lambda_c$ ), we get that  $V_{ab}(T, H) = \pi\xi^2(T)a_0(H)$ , while  $V_c(T, H) = \pi\xi^2(T)d_p$ . As a result, the activation energy of a layered superconductor [Eq. (17)] reads

$$U(T, H) = U(0, H)(1 - T/T_c), \quad (18)$$

where

$$U(0, H) = \frac{A_0}{H^{1/4}}, \quad A_0 = \frac{\Phi_0^2(\Phi_0 d_p^2)^{1/4}}{16\pi\mu_0\gamma\lambda_{ab}^2(0)}. \quad (19)$$

Thus, the above scenario brings about at least a qualitative description of the temperature and field dependences of the activation energy  $U(T, H)$  observed in our own experiments (see Figs. 8 and 9) as well as by other authors.<sup>38,39</sup> Using the experimentally found value of  $U(0, 50G) = 0.5$  eV and taking into account<sup>40</sup> that in  $\text{Bi}_2\text{Sr}_2\text{CaCu}_2\text{O}_8$   $\lambda_{ab}(0) = 2500\text{\AA}$  and  $\gamma = 55$ , Eq. (19) gives for the estimate of the interdefect distance the value

$d_p = 30 \mu\text{m}$  which is quite compatible with an average “grain” size of our textured sample, implying that the motion of “pancake” vortices is indeed limited by weak pinning due to interface boundaries only.

## V. CONCLUSION

In conclusion, by finely measuring the longitudinal magneto-TEP on a textured  $\text{Bi}_2\text{Sr}_2\text{CaCu}_2\text{O}_8$  superconductor, a pronounced field-induced hysteretic behavior of the TEP, due to the difference between cooling and heating runs, has been observed. The hysteresis surface has been found to lie within the interval  $(T_1, T_2)$  around the critical temperature  $T_c$ , with the lower and upper offset temperatures near  $T_1 \approx T_c - 10$  K and  $T_2 \approx T_c + 15$  K, respectively. The field-dependent area of the hysteresis TEP surface,  $A(H)$ , observed has been treated below and above  $T_c$  separately.

The contribution below  $T_c$ ,  $A_{av}(H)$ , has been attributed mainly to the manifestation of the so-called “intrinsic Josephson effect” resulting in Josephson vortices limited behavior of the critical-current density. In so doing the critical-current density is seen to follow the law  $J_c(H) \approx [1 + (H/H_J)^2]^{-1}$ . Above  $T_c$  (but below the upper offset temperature  $T_2$ ), the hysteretic area,  $A_{\bar{h}}(H)$ , has been interpreted mainly in terms of two-dimensional Gaussian fluctuations of the order parameter.

In addition, using an Arrhenius plot of the magneto-TEP below  $T_c$ , the temperature and field dependences of the activation energy,  $U(T, H)$ , have been found to follow the law  $U(T, H) = A_0(1 - T/T_c)/H^{1/4}$ . Such a behavior of the activation energy has been argued to originate from the high anisotropy of the layered superconductor with a preferred direction of flux pinning (due to, e.g., interfaces of textured material or irradiation-induced tracks of columnar defects). Our experimental results give further evidence for the importance of both Abrikosov and Josephson vortex contributions to the transport behavior of the magneto-TEP in layered superconductors.

Finally, it is worthwhile to mention that the TEP hysteresis we have observed was reproducible and practically insensitive to the change of ac heating pulse regimes, indicating a high quality of our textured sample. This is in striking contrast with the analogous measurements of the thermal conductivity on a nontextured ceramic sample, where strong nonequilibrium effects have been observed<sup>48</sup> depending on the ac heating pulse regimes applied.

## ACKNOWLEDGMENTS

Part of this work has been financed through the Incentive Program on High Temperature Superconductors supported by the Belgian State-Prime Minister’s Service-Science Policy Office (SU/02/13). R.C. is a Research Fellow of the FNRS (Brussels).

## APPENDIX

In this appendix, we describe the experimental setup [Figs. 2(a) and 2(b)] and measuring technique in some detail. In Fig. 2,  $BA$  and  $EF$  wires are in constant (Ct)

while  $BC$  and  $ED$  wires are in copper (Cu).  $B$  and  $E$  extremities are spot soldered on a thin (about 3 mm<sup>2</sup> in area) Cu plaquette on the sample. (The plate contact is made according to the suggestion of Conan *et al.*,<sup>49</sup> while the thermocouple positions are disjoined according to the suggestions of Kopp and Slack,<sup>50</sup> who considered in detail the precautions necessary when using thermocouples.)  $A$ ,  $F$ ,  $C$ , and  $D$  extremities are soldered on the Cu block for which the temperature is maintained by a feedback system through heater  $H2$ —this is not usual. The wires are about 20 cm long, and of small cross section in order to increase the thermal resistance toward the ambience; they are wound on the copper block sample holder for thermalization at temperature  $T_0$  measured with a carbon glass resistor (CGR). From the Cu block, and extremities  $ACDF$ , Cu wires lead to precision voltmeters at ambient temperature  $T_a$ , say with wires  $AH$ ,  $CK$ ,  $DG$ , and  $FJ$ , respectively.

Let one measurement be, e.g., with  $T_1 \equiv T_E$ , and  $T_2 \equiv T_B$ ,

$$\begin{aligned} V_{KH} &= V_{KC} + V_{CB} + V_{BA} + V_{AH} \\ &= - \int_{T_0}^{T_a} S_{Cu} dT - \int_{T_2}^{T_0} S_{Cu} dT \\ &\quad - \int_{T_0}^{T_2} S_{Ct} dT - \int_{T_a}^{T_0} S_{Cu} dT, \end{aligned}$$

the first and last terms cancel out, and we have  $V_{KH} = V_{CA} = (S_{Cu} - S_{Ct})(T_2 - T_0)$ , since in the second and third integrals the limits are so close to each other that the functions  $S_{Cu}$  and  $S_{Ct}$  can be considered to be constant in the  $(T_2 - T_0)$  relative interval. The same idea is true for the various potential differences that we are measuring: it is sufficient to consider the potential differences between the leads on the Cu block, and to assume the constancy of the  $S$  functions in the small temperature intervals. Four potential differences can be measured  $V1 = V_D - V_F$ ,  $V2 = V_C - V_A$ ,  $V3 = V_A - V_F$ ,  $V4 = V_C - V_D$  [Fig. 2(b)]. Explicitly, e.g.,

$$\begin{aligned} V3 &= (V_A - V_B) + (V_B - V_E) + (V_E - V_F) \\ &= -S_{Ct}(T_0 - T_2) - S_S(T_2 - T_1) - S_{Ct}(T_1 - T_0), \end{aligned}$$

where  $S_S$  is the TEP of the sample at the appropriate  $(T_2 \approx T_1)$  mean (sample) temperature  $T_S = (T_2 + T_1)/2$  —to be, in fact, self-consistently determined (see below). Some trivial algebra leads to  $V3 = (T_2 - T_1)(S_{Ct} - S_S)$ . Similarly  $V4 = (T_2 - T_1)(S_{Cu} - S_S)$ . The difference  $V4 - V3 = (T_2 - T_1)(S_{Cu} - S_{Ct})$ —the latter difference being a (known from our own calibration table) function of

(the mean) temperature.  $V4 - V3$  is obviously the measure of the temperature gradient on the sample. This being determined, we go back to the measure of  $V4$  to extract the value of  $S_S$ , i.e.,

$$S_S = S_{Cu}(T) - V4 / (T_2 - T_1). \quad (A1)$$

The mean temperature is determined from

$$\begin{aligned} T_S &= (T_2 + T_1) / 2 \\ &= T_0 + (T_1 - T_0) / 2 + (T_2 - T_0) / 2 \end{aligned} \quad (A2)$$

in which the values of  $(T_1 - T_0)$  and  $(T_2 - T_0)$  are given in terms of  $V1$  and  $V2$ , respectively, divided by  $(S_{Cu} - S_{Ct})$ , - which is, in fact, a function of  $T_S$ . An iteration loop is then made starting from  $T_0$  in order to determine the “real”  $T_S$  which is back inserted into the appropriate functions  $(S_{Cu} - S_{Ct})$  and  $S_{Cu}(T)$ .

In fact, we do not measure  $V2$  (which determines  $T_2 - T_0$ ) anymore in order to speed up the acquisition process because  $V2 = V4 - V3 + V1$ .

The thermal run thus goes as follows: we stabilize  $T_0$  through the regulation  $H2$ . The heat flows to the sample through the sample holder and introduces some “residual potential difference” (of the order of 500 nV). All the “residual”  $V_i$ 's are measured at the steady state. The temperature gradient is then applied (during a preprogrammed time at the beginning of the experimental run). It is about 1.0 K. After the steady state is reached the  $V_j$ 's are then measured, and the above calculations made to determine  $T_S$  and  $S_S$ .

Three remarks are still in order. First, the values  $V_j - V_i$  in the above formulas are clearly those corrected for the residual potential difference resulting from the increase of the block temperature (controlled by  $H2$ ) at every step before the gradient of temperature from the heater  $H1$  is imposed. The second remark is crucial to our method: by measuring  $V3$  and  $V4$  we measure the effect of the electrical path through the sample and, in particular, at points  $B$  and  $E$ , and therefore have direct information on the validity of the contacts. (This is, for us, an important test.) The third remark is related to the latter in indicating that  $T_2$ ,  $T_1$ , and  $T_S$  (in fact, their relative values) can be determined from  $V1$  and  $V2$  as well, but such measurements are, in our opinion, less well suited since they bypass the electrical path through the sample, hence the test on the contacts. Finally notice that the Ct-Cu thermocouples are better suited for our (related) study since they are not influenced by a magnetic field, in contrast to Fe-Cu thermocouples.<sup>51</sup>

\*Permanent address: Frank Laboratory of Neutron Physics, Joint Institute for Nuclear Research, 141980 Dubna, Russia.

†Electronic address: U2150MA@BLIULG11.Bitnet

‡Electronic address: 005VVGS@WITSVMA.WITS.AC.ZA

<sup>1</sup>D. K. C. MacDonald, *Thermoelectricity* (Wiley, New York, 1962).

<sup>2</sup>A. B. Kaiser and C. Uher, in *Studies of High Temperature Superconductors*, edited by A. V. Narlikar (Nova Science, New York, 1990), Vol. 7.

<sup>3</sup>V. L. Ginzburg, *Supercond. Sci. Technol.* **4**, S1 (1991); *Usp. Fiz. Nauk.* **161**, 1 (1991) [*Sov. Phys. Usp.* **34**, 101 (1991)].

<sup>4</sup>M. Ausloos, S. K. Patapis, and P. Clippe, in *Physics and Materials Science of High Temperature Superconductors II*, edited by R. Kossowsky, S. Methfessel, D. Wohlleben, and S. K. Patapis (Kluwer, Dordrecht, 1992), p. 755.

<sup>5</sup>S. Martin, A. T. Fiory, R. M. Fleming, G. P. Espinosa, and A. S. Cooper, *Phys. Rev. Lett.* **62**, 677 (1989).

<sup>6</sup>F. Vidal, J. A. Veira, J. Maza, J. J. Ponte, F. Garcia-Alvarado,

- E. Moran, J. Amador, C. Cascales, A. Castro, M. T. Casais, and I. Rasines, *Physica C* **156**, 807 (1988).
- <sup>7</sup>A. Poddar, P. Mandal, A. N. Das, B. Gosh, and P. Chaudhury, *Physica C* **159**, 231 (1989).
- <sup>8</sup>S. K. Patapis, L. Sideridis, G. Apostolopoulos, M. Ausloos, H. L. Luo, C. Politis, T. Puig, M. Pont, J. Munoz, and U. Balachandran, in *Physics and Materials Science of High Temperature Superconductors II*, edited by R. Kossowsky, S. Methfessel, D. Wohlleben, and S. K. Patapis (Kluwer, Dordrecht, 1992), p. 793.
- <sup>9</sup>G. Balestrino, A. Nigro, R. Vaglio, and M. Marinelli, *Phys. Rev. B* **39**, 12264 (1989).
- <sup>10</sup>W. Schnelle, E. Braun, H. Broicher, H. Weiss, H. Geus, S. Ruppel, M. Galfy, W. Braunisch, A. Waldorf, F. Seidler, and D. Wohlleben, *Physica C* **161**, 123 (1989).
- <sup>11</sup>G. Balestrino, M. Marinelli, E. Milani, L. Reggiani, R. Vaglio, and A. A. Varlamov, *Phys. Rev. B* **46**, 14919 (1992).
- <sup>12</sup>O. Cabeza, Y. P. Yadava, J. Maza, F. Vidal, F. Garcia-Alvarado, M. A. Senaris-Rodriguez, A. Varez, and E. Moran, *Physica C* **185-189**, 11897 (1991).
- <sup>13</sup>P. De Villiers, R. A. Doyle, and V. V. Gridin, *J. Phys.: Condens. Matter* **4**, 9401 (1992).
- <sup>14</sup>V. V. Gridin and R. A. Doyle, *Phys. Scr.* **46**, 381 (1992).
- <sup>15</sup>N. V. Zavaritsky, A. V. Samoilov, and A. A. Yurgens, *Physica C* **180**, 419 (1991).
- <sup>16</sup>N. V. Zavaritsky, A. V. Samoilov, and A. A. Yurgens, *Pis'ma Zh. Eksp. Teor. Fiz.* **55**, 133 (1992) [*JETP Lett.* **55**, 127 (1992)].
- <sup>17</sup>V. V. Gridin, P. Permambuco-Wise, C. G. Trendall, W. R. Datars, and J. D. Garrett, *Phys. Rev. B* **40**, 8814 (1989).
- <sup>18</sup>A. A. Varlamov and D. V. Livanov, *Zh. Eksp. Teor. Fiz.* **98**, 584 (1990) [*Sov. Phys. JETP* **71**, 325 (1990)].
- <sup>19</sup>S. A. Sergeenkov, V. V. Gridin, P. de Villiers, and M. Ausloos (unpublished).
- <sup>20</sup>S. A. Sergeenkov, *J. Supercond.* **3**, 417 (1990).
- <sup>21</sup>A. V. Ustinov, M. Hartmann, R. P. Huebener, G. Yu. Logvenov, and V. V. Ryazanov, *Supercond. Sci. Technol.* **4**, 5400 (1991).
- <sup>22</sup>R. P. Huebener, A. V. Ustinov, and V. V. Kaplunenko, *Phys. Rev. B* **42**, 4831 (1990).
- <sup>23</sup>R. P. Huebener, F. Kober, R. Gross, and H. C. Ri, *Physica C* **185-189**, 349 (1991).
- <sup>24</sup>C. Hohn, M. Galfy, A. Dascoulidou, A. Freimuth, H. Soltner, and U. Poppe, *Z. Phys. B* **85**, 161 (1991).
- <sup>25</sup>R. A. Doyle, Ph.D. thesis, University of Witwatersrand, 1992.
- <sup>26</sup>Ch. Laurent, H. W. Vanderschueren, A. Rulmont, P. Tarte, and M. Ausloos, *Appl. Phys. Lett.* **52**, 1179 (1988).
- <sup>27</sup>M. Ausloos, Ch. Laurent, S. K. Patapis, A. Rulmont, and P. Tarte, *Mod. Phys. Lett. B* **3**, 167 (1989).
- <sup>28</sup>L. Bulaevskii, J. Clem, and L. Glazman, *Phys. Rev. B* **46**, 350 (1992).
- <sup>29</sup>R. Kleiner, F. Steinmeyer, G. Kunkel, and P. Muller, *Phys. Rev. Lett.* **68**, 2394 (1992).
- <sup>30</sup>J. Bock and E. Preisler, *Solid State Commun.* **72**, 453 (1989).
- <sup>31</sup>Ch. Laurent, S. K. Patapis, H. W. Vanderschueren, A. Rulmont, P. Tarte, and M. Ausloos, *Solid State Commun.* **66**, 445 (1988).
- <sup>32</sup>M. F. Crommie, A. Y. Liu, M. L. Cohen, and A. Zettl, *Phys. Rev. B* **41**, 2526 (1990).
- <sup>33</sup>L. M. Leon and R. Escudero, *Physica B* **165&166**, 1211 (1990).
- <sup>34</sup>H. E. Stanley, *Introduction to Phase Transitions and Critical Phenomena* (Clarendon, Oxford, 1968), Chap. 7.
- <sup>35</sup>M. E. Fisher and J. S. Langer, *Phys. Rev. Lett.* **20**, 665 (1968).
- <sup>36</sup>W. J. Skocpol and M. Tinkham, *Rep. Prog. Phys.* **38**, 1049 (1975).
- <sup>37</sup>V. V. Gridin, T. W. Krause, and W. R. Datars, *J. Appl. Phys.* **68**, 675 (1990).
- <sup>38</sup>T. T. M. Palstra, B. Batlogg, L. F. Schneemeyer, and J. V. Waszczak, *Phys. Rev. Lett.* **61**, 1662 (1988); **64**, 3090 (1990).
- <sup>39</sup>A. Dascoulidou, M. Galfy, C. Hohn, N. Knauf, and A. Freimuth, *Physica C* **201**, 202 (1992).
- <sup>40</sup>D. R. Harshman and A. P. Mills, Jr., *Phys. Rev. B* **45**, 10684 (1992).
- <sup>41</sup>J. R. Clem, *Phys. Rev. B* **43**, 7837 (1991).
- <sup>42</sup>A. Barone and G. Paterno, *Physics and Applications of the Josephson Effect* (Wiley, New York, 1982), Chap. 4.
- <sup>43</sup>W. Gerhauser, G. Ries, H. W. Neumuller, W. Schmidt, O. Eibl, G. Saemann-Ischenko, and S. Klaumunzer, *Phys. Rev. Lett.* **68**, 879 (1992).
- <sup>44</sup>R. P. Huebener, *Magnetic Flux Structures in Superconductors* (Springer-Verlag, Berlin, 1979).
- <sup>45</sup>D. E. Farrell, S. Bonham, J. Foster, Y. C. Chang, P. Z. Jiang, K. G. Vandervoort, D. L. Lam, and V. G. Kogan, *Phys. Rev. Lett.* **63**, 782 (1989).
- <sup>46</sup>M. Tinkham, *Phys. Rev. Lett.* **61**, 1658 (1988).
- <sup>47</sup>J. T. Kucera, T. P. Orlando, G. Virshup, and J. N. Eckstein, *Phys. Rev. B* **46**, 11004 (1992).
- <sup>48</sup>H. Bougrine, S. Sergeenkov, M. Ausloos, R. Cloots, and V. V. Gridin (unpublished).
- <sup>49</sup>A. Conan, G. Coureaux, and M. Zoater, *J. Phys. Appl.* **6**, 383 (1971).
- <sup>50</sup>J. Kopp and G. A. Sloack, *Cryogenics* **11**, 22 (1971).
- <sup>51</sup>See note in last paragraph of H. H. Sample, L. J. Neuringer, and L. G. Rubin, *Rev. Sci. Instrum.* **45**, 64 (1974).

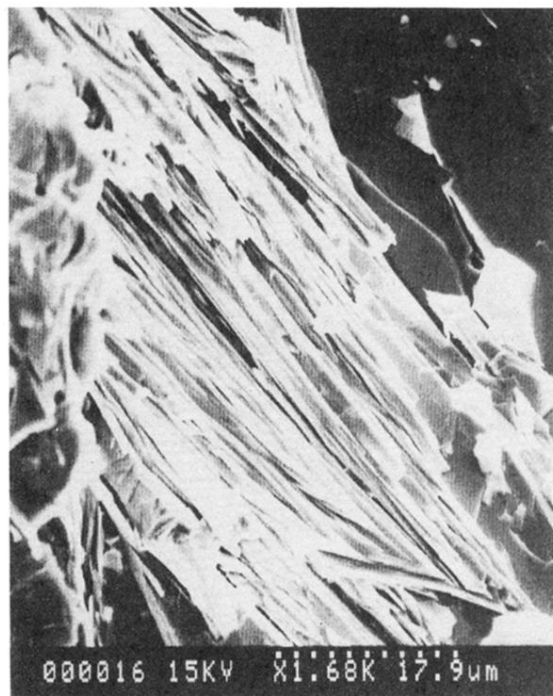


FIG. 1. Scanning electron micrograph of the textured  $\text{Bi}_2\text{Sr}_2\text{CaCu}_2\text{O}_8$  sample.